Computer-Aided Design of Evanescent-Mode Waveguide Filter with Nontouching *E*-Plane Fins

QIU ZHANG AND TATSUO ITOH, FELLOW, IEEE

Abstract—**This paper presents a computer-aided design algorithm for the analysis and design of an evanescent-mode bandpass filter with nontouching *E*-plane fins. The theoretical analysis is based on the generalized scattering matrix technique in conjunction with the spectral-domain approach and mode-matching method. The technique used in this paper takes into account the dominant as well as the higher order effects. The measured filter responses in the *Ka*-band are in good agreement with those obtained by this analysis.**

I. INTRODUCTION

IN THE LATE 1950's Jaynes [1] and Edson [2] proposed that resonators built in a cutoff waveguide may be used in filter design. These filters are called evanescent-mode filters. Microwave bandpass filters using evanescent modes have been designed successfully [3]–[5]. The evanescent-mode bandpass filter has several advantages over the conventional type of bandpass filters (waveguide above cutoff, coaxial line, etc.). For instance, a sharper transition to out-of-band rejection can be obtained on the higher frequency side. Evanescent-mode waveguide filters are also smaller than traditional waveguide filters. A waveguide operating below its cutoff frequency is basically an inductive element [5], [6]. Suitable capacitive elements are needed to construct an evanescent-mode waveguide bandpass filter. Evanescent-mode filters using conventional capacitive elements such as tuning screws [4], [5] are costly and difficult to mass-produce because of their complicated structure.

Nontouching *E*-plane fins [7], which are easily fabricated, are proposed in this study as the capacitive elements. The filter structure, shown in Fig. 1, consists of a number of nontouching *E*-plane fins placed in a rectangular waveguide below cutoff. The fins may be metal only or supported by a dielectric layer. The input and output portions of the filter are coupled to the external circuits via double-step waveguide junctions. The larger waveguides operate above the cutoff frequency. Since the capacitive elements utilize a printed circuit structure, they are suitable for mass production at low cost.

The initial approach to the synthesis of an evanescent-mode filter was based on image parameter theory [3].

Manuscript received April 15, 1987; revised September 23, 1987. This work was supported in part by the U.S. Army Research Office under Contract DAAG-29-84-K-0076.

The authors are with the Department of Electrical and Computer Engineering, University of Texas at Austin, Austin, TX 78712.

IEEE Log Number 8717985.

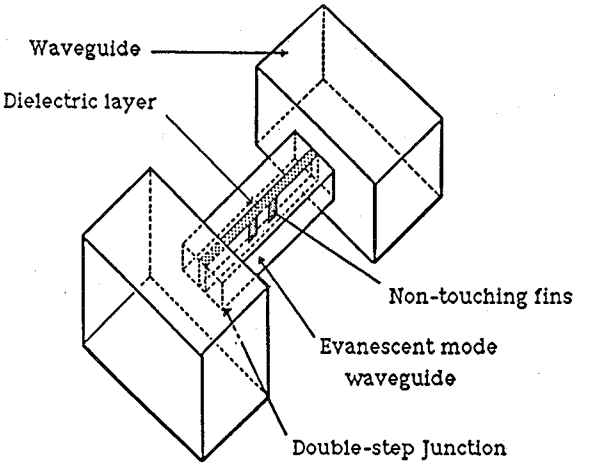

Fig. 1. The structure of evanescent-mode waveguide filter with nontouching *E*-plane fins.

Recently a design theory based on the equivalent circuit analysis was used by Craven and Mok [4]. The basic assumption used is that the only mode existing in the guide is an evanescent TE_{10} mode. Under this assumption a simple transmission line equivalent circuit is applicable. The filter then can be represented by an equivalent circuit of the coupled resonators [8], [9]. Although this technique is accurate enough for some designs, the equivalent circuit approach neglects the effects of higher order modes. Omission of these effects could cause a bandwidth shrinkage and higher bandpass ripples in the filter response. In this paper a generalized scattering matrix technique is used in conjunction with the spectral-domain approach and the mode-matching method to analyze and design an evanescent-mode waveguide bandpass filter with nontouching *E*-plane fins. This method takes into account the effect of the dominant as well as all the higher order modes.

As shown in Figs. 1 and 2, the filter consists of three portions: the double-step waveguide junctions; the nontouching *E*-plane fin portion, which may contain more than one fin; and the waveguide below cutoff. First each portion is characterized by its corresponding generalized scattering matrix. In this study, the scattering matrix of the double-step junction is found by the mode-matching technique. The scattering matrix of the nontouching fin is obtained by combining the spectral-domain method with

0018-9480/88/0200-0404$01.00

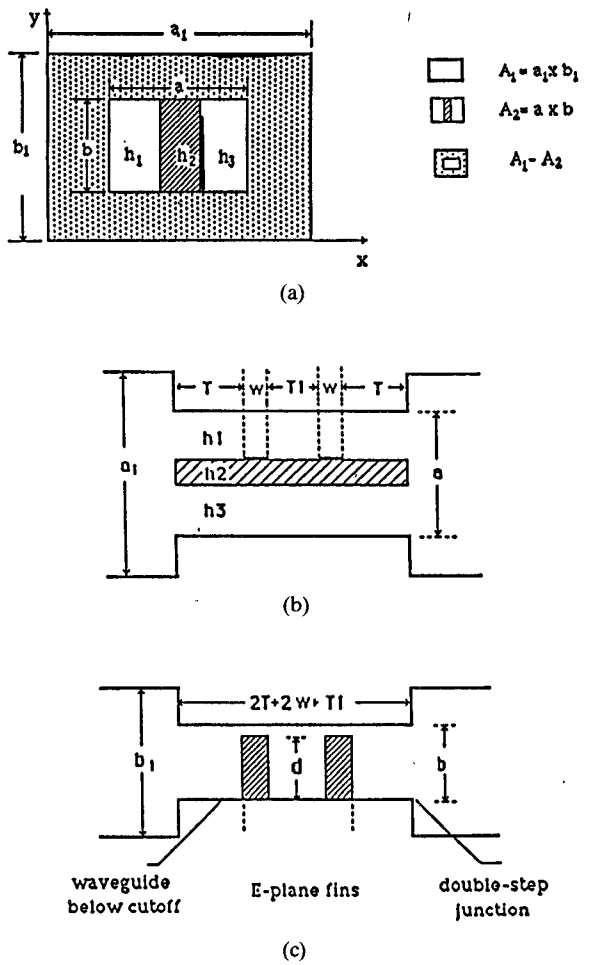

Fig. 2. (a) Cross sectional view. (b) Top view. (c) Side view of the filter.

residue calculus [7]. The scattering matrix of the evanescent waveguide is derived by the transmission line equivalent circuits of the waveguide. These matrices are then combined via a generalized scattering matrix technique to obtain the scattering matrix description of the evanescent-mode filter. The insertion loss and the return loss of the filter can then be obtained from the final scattering matrix.

Filters designed with the present technique have been tested in the *Ka*-band. Good agreement between theory and measurement is observed.

II. Analysis and Design Procedure

The analysis of an evanescent-mode waveguide bandpass filter with nontouching *E*-plane fin is based on the generalized scattering matrix technique in conjunction with the spectral-domain approach and the mode-matching method. The study begin with a brief description of the generalized scattering matrix. Then the scattering matrix representations for the double-step junction, the nontouching *E*-plane fins, and the evanescent-mode waveguide section are obtained by the mode-matching technique, the spectral-domain method, and waveguide theory, respectively. Finally, these scattering matrices are combined to obtain the final generalized scattering matrix. The filter response is calculated from the final scattering matrix.

A. Generalized Scattering Matrix

The concept of a generalized scattering matrix, introduced by Pace and Mittra [10], is closely related to the scattering matrix of circuit theory or of microwave network theory. It differs by including scattering of all modes, so that the scattering matrix will in general be of infinite order.

The scattering matrix can be defined for a junction discontinuity at which the fields may be expanded in modes, such as the double-step waveguide junction. Consider that the *mn*th TE mode is incident upon the plane $z = 0$ from the larger waveguide I and waves are reflected back into waveguide I and transmitted into the smaller waveguide II. If the amplitude of the *mn*th TE incident in I is normalized to unity, then the amplitude of the *pq*th TE scattered mode in waveguide I is $S_{\mathrm{II}}^{\mathrm{EE}}(pq, mn)$, and the amplitude of the *pq*th transmitted TM mode in waveguide II is $S_{\mathrm{III}}^{\mathrm{ME}}(pq, mn)$.

In the notation used above, the scattering matrix relates the excited modes to the incident ones via

$$\begin{pmatrix} A^s \\ B^s \end{pmatrix} = [S_d] \begin{pmatrix} A^i \\ B^i \end{pmatrix} \tag{1}$$

The superscript s indicates scattered fields, and i expresses the incident fields. The general element of S_d is $S_{ij}^{xy}(pq, mn)$, where x and y (= E or M) represent a TE or TM to z wave; i and j = I or II indicate the larger guide or smaller guide; m, n, p, and q are integers corresponding to different modes. Theoretically the generalized matrix is of infinite dimensions corresponding to the infinite number of eigenmodes. The matrix is truncated to finite size for numerical calculations [11].

B. Scattering Matrix Representation of a Double-Step Junction by Mode-Matching Method

In this section the scattering matrix representation of a double-step junction is derived via the mode-matching technique [12], [13]. We use I to represent the larger guide while the smaller guide, which is a partially dielectric-loaded waveguide, is denoted by II. The field is derived from the electric vector potential $\boldsymbol{F}$ and the magnetic vector potential $\boldsymbol{A}$ [14]:

$$\boldsymbol{E} = -\nabla \times \boldsymbol{F} + \nabla \times \nabla \times \boldsymbol{A}/j\omega\epsilon_0 \tag{2}$$

$$\boldsymbol{H} = \nabla \times \boldsymbol{A} + \nabla \times \nabla \times \boldsymbol{F}/j\omega\mu_0. \tag{3}$$

In this study it is convenient to choose

$$\boldsymbol{A} = \psi \boldsymbol{x} \tag{4}$$

$$\boldsymbol{F} = \phi \boldsymbol{x} \tag{5}$$

where ϕ and ψ are the scalar functions which represent the electric (TE) wave and magnetic (TM) wave transverse to the x direction, respectively, and $\boldsymbol{x}$ is a vector in the x direction. These potentials are extended in terms of their eigenfunctions, which must satisfy the boundary conditions. The potentials in each region can be expressed as

follows:

$$\phi_i = \sum_{m=1}^{M}\sum_{n=0}^{N}\left[a_{imn}\exp(-k_{izhmn}z) + b_{imn}\exp(k_{izhmn}z)\right]P_{imn}(x,y) \quad (6)$$

$$\psi_i = \sum_{m=0}^{M}\sum_{n=1}^{N}\left[c_{imn}\exp(-k_{izemn}z) + d_{imn}\exp(k_{izemn}z)\right]Q_{imn}(x,y). \quad (7)$$

The notation used in this part is as follows:

X_{icjdl}
- $l = m, n$, or mn indicates mth, nth, or mnth mode;
- $d = h$ or e, h: TE-to-x field; e: TM-to-x field;
- $j = 1$, 2, or 3 indicates the variable in the region 1, 2, or 3 of the smaller waveguide;
- $c = x$, y, or z indicates that x, y, or z direction, respectively;
- $i = \mathrm{I}$ or II, I: larger waveguide; II: smaller waveguide;
- indicates the variable

where

$$P_{imn}(x,y) = R_{im}(x)S_{in}(y) \quad (8)$$

$$Q_{imn}(x,y) = T_{im}(x)V_{in}(y) \quad (9)$$

are the eigenfunctions of the TE-to-x and TM-to-x fields, respectively. In region I, these eigenfunctions are represented by

$$R_{\mathrm{I}m}(x) = N_{r\mathrm{I}m}\sin(m\pi x/a_1) \quad (10)$$

$$S_{\mathrm{I}n}(y) = N_{s\mathrm{I}n}\cos(n\pi y/b_1) \quad (11)$$

$$T_{\mathrm{I}m}(x) = N_{t\mathrm{I}m}\cos(m\pi x/a_1) \quad (12)$$

$$V_{\mathrm{I}n}(y) = N_{v\mathrm{I}n}\sin(n\pi y/b_1) \quad (13)$$

$$m = 0,1,2,\cdots,M; \qquad n = 0,1,2,\cdots,N.$$

In the smaller waveguide, the eigenfunctions are given by

$$S_{\mathrm{II}q}(y) = N_{s\mathrm{II}q}\cos[(q\pi/b)(y-y_1)] \quad (14)$$

$$R_{\mathrm{II}p}(x) = \begin{cases} N_{r\mathrm{II}1p}\sin k_{\mathrm{II}x1hp}(x-x_1) & x_1 < x < x_1+h_1 \\ N_{r\mathrm{II}2p}\sin k_{\mathrm{II}x2hp}(x-x_1-h_1) & \\ \quad + \bar{N}_{r\mathrm{II}2p}\cos k_{x\mathrm{II}2hp}(x-x_1-h_1) & x_1+h_1 < x < x_1+h_1+h_2 \\ N_{r\mathrm{II}3p}\sin k_{\mathrm{II}x}D3_{hp}(x-x_1-a) & x_1+h_1+h_2 < x < x_1+a \end{cases} \quad (15)$$

$$V_{\mathrm{II}q}(y) = N_{v\mathrm{II}q}\sin[(q\pi/b)(y-y_1)] \quad (16)$$

$$T_{\mathrm{II}p}(x) = \begin{cases} N_{t\mathrm{II}1p}\cos k_{\mathrm{II}x1ep}(x-x_1) & x_1 < x < x_1+h_1 \\ N_{t\mathrm{II}2p}\cos k_{\mathrm{II}x2ep}(x-x_1-h_1) & \\ \quad + \bar{N}_{t\mathrm{II}2p}\sin k_{\mathrm{II}x2ep}(x-x_1-h_1) & x_1+h_1 < x < x_1+h_1+h_2 \\ N_{t\mathrm{II}3p}\cos k_{\mathrm{II}x3p}(x-x_1-a) & x_1+h_1+h_2 < x < x_1+a \end{cases} \quad (17)$$

$$p = 0,1,2,\cdots,P; \qquad q = 0,1,2,\cdots,Q.$$

where $N_{r\mathrm{I}m}$, $N_{t\mathrm{I}n}$, $N_{r\mathrm{II}jp},\cdots$, and $N_{t\mathrm{II}jq}$, are normalized coefficients. The mth eigenmodes of TE-to-x and TM-to-x fields in the partially filled waveguide in region j are represented by $k_{\mathrm{II}xjhm}$ and $k_{\mathrm{II}xjem}$. Here k_{izhmn} and k_{izemn} are the propagation constants of the mnth TE- and TM-to-x fields in the x direction, and must satisfy the following dispersion equations:

$$(k_{\mathrm{I}zdmn})^2 + k_0^2 = (m\pi/a_1)^2 + (n\pi/b_1)^2 \quad (18)$$

$$(k_{\mathrm{II}zdmn})^2 + k_j^2 = (k_{\mathrm{II}xjdm})^2 + (n\pi/b)^2 \quad (19)$$

where $d = h$ or e, $j = 1$, 2, and 3, k_0 is the wavenumber in free space, $k_j = \sqrt{\epsilon_j}k_0$, and ϵ_j is the relative dielectric constant of the smaller guide in region j. The coefficients a_{imn}, b_{imn}, c_{imn}, and d_{imn} in (6) and (7) correspond to incident and reflected waves and are related to each other by the scattering matrix. The scattering matrix can be determined by matching the tangential fields at the step discontinuity at $z = 0$ (see Fig. 2(a)):

$$\begin{aligned} &E_{\mathrm{I}x,y|\text{at } z=0} = E_{\mathrm{II}x,y|\text{at } z=0} && \text{in area } A_2 \\ &H_{\mathrm{I}x,y|\text{at } z=0} = H_{\mathrm{II}x,y|\text{at } z=0} && \text{in area } A_2 \\ &E_{\mathrm{I}x,y|\text{at } z=0} = 0 && \text{in area } A_1 - A_2. \end{aligned} \quad (20)$$

Applying the orthogonality relationship between potential functions leads to the matrix equation

$$\underbrace{\begin{pmatrix} \boldsymbol{Ma}_{\mathrm{I}} & \mathbf{0} & -\boldsymbol{V}_{b\mathrm{II}} & \mathbf{0} \\ \mathbf{0} & \boldsymbol{V}_{c\mathrm{I}} & \mathbf{0} & -\boldsymbol{M}_{d\mathrm{II}} \\ \boldsymbol{M}_{b\mathrm{I}} & \boldsymbol{M}_{c\mathrm{I}} & -\boldsymbol{V}_{a\mathrm{II}} & \boldsymbol{V}_{d\mathrm{II}} \\ \boldsymbol{V}_{a\mathrm{I}} & -\boldsymbol{V}_{d\mathrm{I}} & \boldsymbol{M}_{b\mathrm{II}} & \boldsymbol{M}_{c\mathrm{II}} \end{pmatrix}}_{\boldsymbol{M}_1} \begin{pmatrix} \boldsymbol{A}_{\mathrm{I}mn} \\ \boldsymbol{C}_{\mathrm{I}mn} \\ \boldsymbol{B}_{\mathrm{II}pq} \\ \boldsymbol{D}_{\mathrm{II}pq} \end{pmatrix} = \underbrace{\begin{pmatrix} -\boldsymbol{M}_{a\mathrm{I}} & \mathbf{0} & \boldsymbol{V}_{b\mathrm{II}} & \mathbf{0} \\ \mathbf{0} & -\boldsymbol{V}_{c\mathrm{I}} & \mathbf{0} & \boldsymbol{M}_{d\mathrm{II}} \\ -\boldsymbol{M}_{b\mathrm{I}} & \boldsymbol{M}_{c\mathrm{I}} & \boldsymbol{V}_{a\mathrm{II}} & \boldsymbol{V}_{d\mathrm{II}} \\ \boldsymbol{V}_{a\mathrm{I}} & \boldsymbol{V}_{d\mathrm{I}} & \boldsymbol{M}_{b\mathrm{II}} & -\boldsymbol{M}_{c\mathrm{II}} \end{pmatrix}}_{\boldsymbol{M}_2} \begin{pmatrix} \boldsymbol{B}_{\mathrm{I}mn} \\ \boldsymbol{D}_{\mathrm{I}mn} \\ \boldsymbol{A}_{\mathrm{II}pq} \\ \boldsymbol{C}_{\mathrm{II}pq} \end{pmatrix}$$

where $\boldsymbol{M}_{a\mathrm{I}}$, $\boldsymbol{M}_{c\mathrm{I}}$, etc, express matrices. For instance, $\boldsymbol{M}_{a\mathrm{I}}$ is a matrix of dimensions $P \times Q \times M \times N$. $\boldsymbol{V}_{b\mathrm{II}}, \boldsymbol{V}_{a\mathrm{I}}, \cdots$ are diagonal matrix of dimensions $P \times Q \times P \times Q$, $M \times N \times M \times N, \cdots$, and $\boldsymbol{A}_{mn}, \boldsymbol{D}_{pq}, \cdots$ etc. are vectors of dimensions $M \times N$ or $P \times Q$.

The scattering matrix of the double-step discontinuity is then given by

$$\boldsymbol{S}_d = \begin{pmatrix} \boldsymbol{S}_{d11} & \boldsymbol{S}_{d12} \\ \boldsymbol{S}_{d21} & \boldsymbol{S}_{d22} \end{pmatrix} = \boldsymbol{M}_2^{-1}\cdot\boldsymbol{M}_1. \quad (21)$$

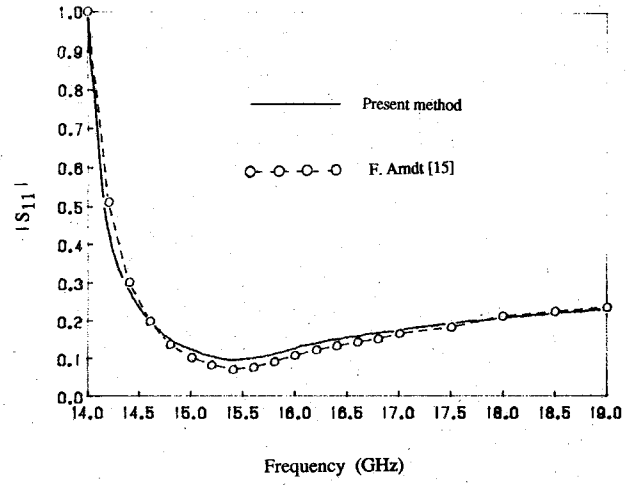

Fig. 3. Reflection coefficient $|S_{11}|$ as a function of frequency if a TE_{10} wave is incident from *Ku*-band waveguide (15.8×7.9 mm^2) to *K*-band guide (10.7×4.32 mm^2).

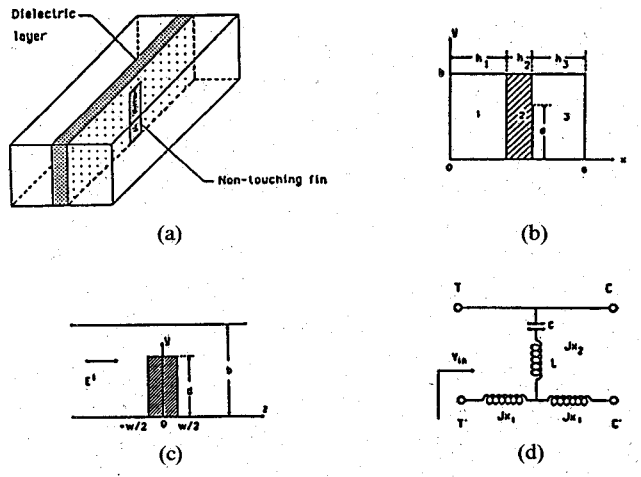

Fig. 4. (a) Nontouching *E*-plane fin in a rectangular waveguide. (b) End view. (c) Side view. (d) Equivalent circuit of the nontouching fin.

Since the double-step junction is between an empty waveguide and a partially filled waveguide, the formulation is much more complicated than a simple double-step junction. The program was checked by computing the scattering parameters of a simple double-step waveguide discontinuity from *Ku*- to *K*-band (15.8 mm$\times$7.9 mm to 10.7 mm$\times$4.32 mm) with $M=8$, $N=4$, $P=5$, and $Q=2$. The results are in good agreement results with Arndt and Wriedt's (Fig. 3) [15].

C. Matrix Representation for the Portion of Nontouching Fins

The scattering matrix for a nontouching fin can be obtained by combining the spectral domain method with residue calculus [7]. A brief description is given here, since more details can be found in [7]. Referring to Fig. 4 at $x=h_1+h_2$, the sum of the incident fields (E_y^i and E_z^i) and the scattering fields (E_y^S and E_z^S) must be equal to the total fields (E_y^t and E_z^t). In the space-domain formulation, coupled integral equations for the unknown current distributions j_y and j_z on the strip, which generates the scattered fields, may be derived from the condition that the total of the tangential fields must be equal to zero on the strip. In the Fourier transform domain defined by

$$\tilde{\psi}(\alpha_n,\beta)=\int \exp(j\alpha_n y)\,dy\int\psi(y,z)\exp(j\beta_z)\,dz \quad (22)$$

$$\alpha_n=n\pi/b$$

the above statement is

$$\tilde{E}^S=\tilde{E}^t-\tilde{E}^i=\tilde{G}_{yy}\tilde{J}_y+\tilde{G}_{yz}\tilde{J}_z \quad (23)$$

$$\tilde{E}^S=\tilde{E}^t-\tilde{E}^i=\tilde{G}_{z_y}\tilde{J}_y+\tilde{G}_{zz}\tilde{J}_z \quad (24)$$

where $\tilde{G}_{yy}$ etc. are Fourier transforms of dyadic Green's function. A set of inhomogeneous algebraic equations can be obtained by applying Galerkin's method to (23) and (24):

$$\sum_i^I K_{pi}^{yy}a_i+\sum_j^J K_{pj}^{yz}b_j=-\langle\tilde{J}_{yp}^*,\tilde{E}_y^i\rangle,\qquad p=1,2,\cdots,I \quad (25)$$

$$\sum_i^I K_{qi}^{zy}a_i+\sum_j^J K_{qj}^{zz}b_j=-\langle\tilde{J}_{zq}^*,\tilde{E}_z^i\rangle,\qquad q=1,2,\cdots,J \quad (26)$$

where $\langle\ \rangle$ indicates the inner product and * denotes the complex conjugate. Note that, in contrast to the eigenvalue problem, the right-hand sides of (25) and (26) are not zero because the contribution of the incident field is nonzero everywhere. Equations (25) and (26) are solved for the expansion coefficeints a_i and b_i of the assumed current distribution $j_y=\Sigma_i^I a_i j_{yi}$ and $j_z=\Sigma_j^J b_j j_{zj}$. Hence $\tilde{E}_y^S$ and $\tilde{E}_z^S$ are now completely known from (23) and (24).

On the other hand, the scattered field for $|z|>w/2$ can be expanded into LSE and LSM modes containing propagation factors such as $\exp(\pm j\beta_{mn}z)$ in the space domain. Hence in the spectral domain, they are expanded in the series containing such pole terms as $1/(\beta\pm\beta_{mn})$, where the β_{mn} are the propagation constants of the LSE and LSM modes. The left-hand sides of (23) and (24) can be written in terms of these series expansions with unknown modal amplitudes, which are related to the scattering parameters of the generalized scattering matrix. Note that $\tilde{G}_{yy}$ etc. contain poles at $\pm\beta_{mn}$. Hence, the modal amplitudes can be found by equating the residue of both sides of (23) or (24), namely, the scattering matrix of the nontouching fin can be determined.

Since the filter may contain more than one fin element, a general case must be considered here. Fig. 5 shows a structure consisting of n fins, which are indicated by $F_1, F_2,\cdots, F_n$. These fins are separated from one to another by distances $T_1, T_2,\cdots, T_{n-1}$. To obtain a scattering matrix representation $\boldsymbol{S}$ for this portion, we consider that a substructure which consists of fins F_1 and F_2, with spacing T_1. The substructure is shown in Fig. 6. The scattering matrices of fins F_1 and F_2, $\boldsymbol{S}_{f1}$ and $\boldsymbol{S}_{f2}$ are obtained by the method described above. With the scattering matrix notation, each of these matrices contains four submatrices

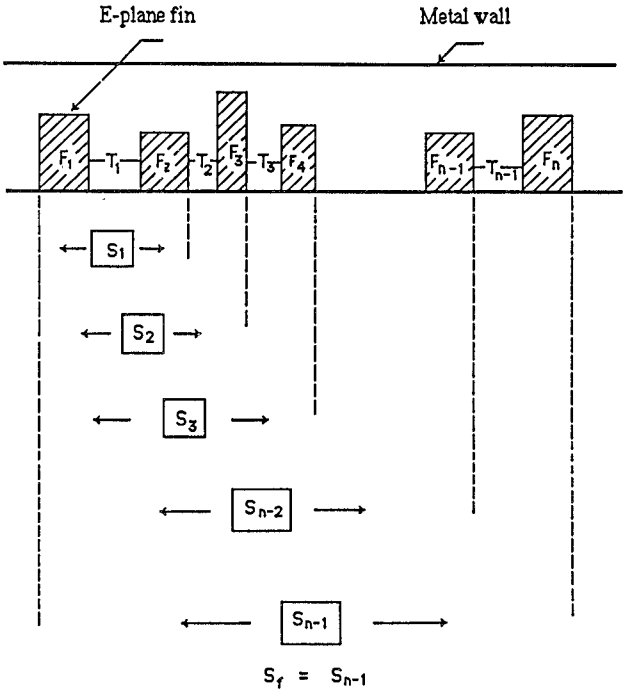

Fig. 5. A filter containing n nontouching fins.

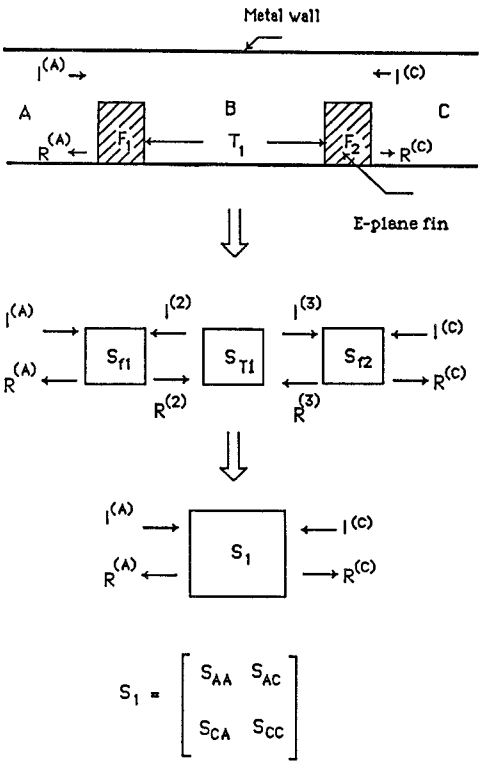

Fig. 6. Derivation of scattering matrix for the cascaded substructure.

and can be written as

$$S_{f1} = \begin{pmatrix} S_{f111} & S_{f112} \\ S_{f121} & S_{f122} \end{pmatrix} \tag{27}$$

$$S_{f2} = \begin{pmatrix} S_{f211} & S_{f212} \\ S_{f221} & S_{f222} \end{pmatrix}. \tag{28}$$

With the knowledge of the scattering parameters for a single fin, the generalized scattering matrix technique is applied to obtain a scattering matrix of this substructure. The concept is that of multiple-reflection phenomenon. If a wave from region A is incident upon F_1, fields will be partly reflected back into region A and partly transmitted into region B. After traveling a distance T_1, a part of the wave transmitted into region B is reflected back and the remaining part is transmitted into region C via F_2. This process continues until the reflected wave dies out. This multiple-reflection phenomenon between F_1 and F_2 implies a matrix combination process that leads to the scattering matrix for the substructure.

In region B of Fig. 6, the smaller waveguide section with length T_1, operated below its cutoff frequency, is represented by the matrix S_{T1}. The elements of those matrices are easily obtained from the transmission line equivalent circuits of the guide, in which the characteristic impedances are imaginary. Since no propagation modes exist below the cutoff frequency, this waveguide section in the equivalent circuit acts as a lumped reactance. The wave "travels" a distance $T1$ in this guide, so each mode is multiplied by an exponential decay factor $\exp(-\kappa_{\text{II}zdmn}T_1)$, where $d = h$ or e represent TE or TM waves, respectively. In more detail, S_{T1} can be written as

$$S_{T1} = \begin{pmatrix} \mathbf{0} & S_{t1} \\ S_{t1} & \mathbf{0} \end{pmatrix} \tag{29}$$

where the submatrix S_{t1} is given by

$$S_{t1} = \begin{pmatrix} \exp(-\kappa_{\text{II}zh10}T_1) & 0 & \cdots & 0 \\ 0 & \exp(-\kappa_{\text{II}zh20}T_1) & & \vdots \\ \vdots & & \exp(-\kappa_{\text{II}ze01}T_1) & \\ 0 & \cdots & 0 & \exp(-\kappa_{\text{II}zePQ}T_1) \end{pmatrix}. \tag{30}$$

The combination of S_{t1} with S_{f1} and S_{f2} results in the scattering matrix S_1 in Fig. 5 that represents the cascaded structure. The elements of matrix S_1 in Fig. 5 are given by

$$S_{AA} = S_{f111} + S_{f112}S_{t1}U_2S_{f211}S_{t1}S_{f121} \tag{31}$$

$$S_{AC} = S_{f112}S_{t1}U_2S_{f212} \tag{32}$$

$$S_{CA} = S_{f221}S_{t1}U_1S_{f121} \tag{33}$$

$$S_{CC} = S_{f222} + S_{f221}S_{t1}S_{f122}S_{t1}S_{f212} \tag{34}$$

$$U_1 = (I - S_{f122}S_{t1}S_{f211}S_{t1})^{-1} \tag{35}$$

$$U_2 = (I - S_{f211}S_{t1}S_{f122}S_{t1})^{-1} \tag{36}$$

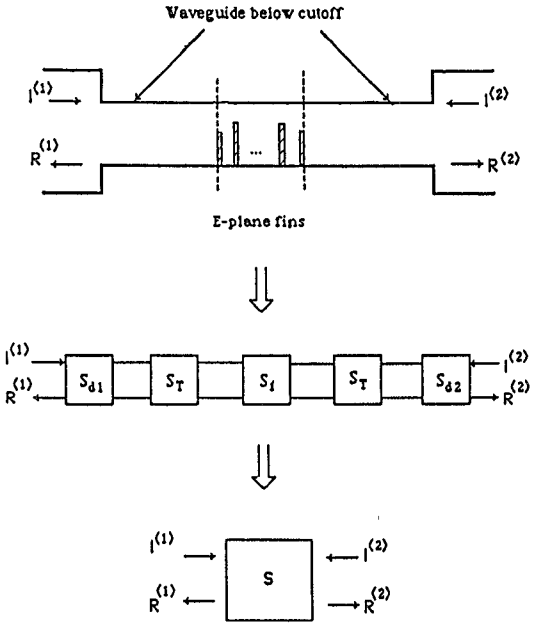

Fig. 7. Derivation of the final scattering matrix for the filter structure.

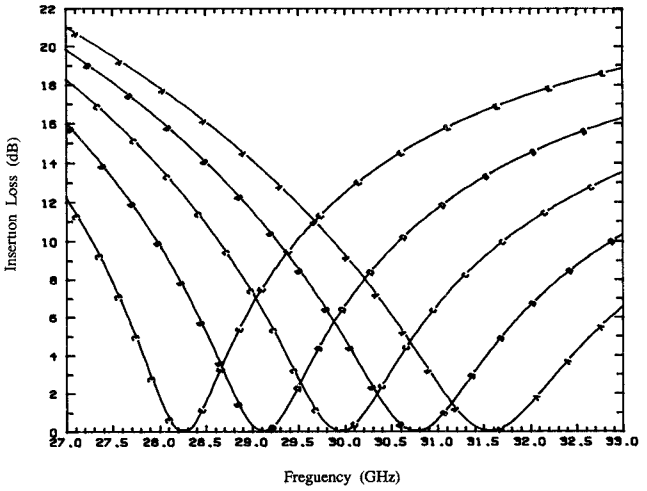

Fig. 8. Insertion loss of the filter versus frequency for different heights d of the E-plane fin. $h_1 = 1.753$ mm; $h_2 = 0.127$ mm; $\epsilon_2 = 2.2$ $w = 0.3$ mm; $T = 2.0$ mm; $A: d = 1.4$ mm; $B: d = 1.45$ mm; $C: d = 1.50$ mm; $D: d = 1.55$ mm; $E: d = 1.60$ mm.

where $\boldsymbol{I}$ is the identity matrix. In the next step, we consider the substructure that consists of fins F_1, F_2, and F_3 with spacing T_1 and T_2. The combination of F_1, F_2, and T_1 is now expressed by matrix $\boldsymbol{S}_1$. Using $\boldsymbol{S}_{T2}$ and $\boldsymbol{S}_{f3}$ to represent scattering matrices of T_2 and F_3 respectively, we obtain the matrix $\boldsymbol{S}_2$ of this substructure in the same way as that of deriving matrix $\boldsymbol{S}_1$. The same procedure is repeated until the matrix $\boldsymbol{S}_f$ is obtained (Fig. 5).

D. Scattering Matrix Representations of Cascaded Sections

The side view of the filter can be now represented by Fig. 7. The double-step junctions are described by scattering matrices $\boldsymbol{S}_{d1}$ and $\boldsymbol{S}_{d2}$. The capacitive element of the filter is the portion of the nontouching E-plane fins, which is represented by scattering matrices $\boldsymbol{S}_f$. The matrices $\boldsymbol{S}_T$

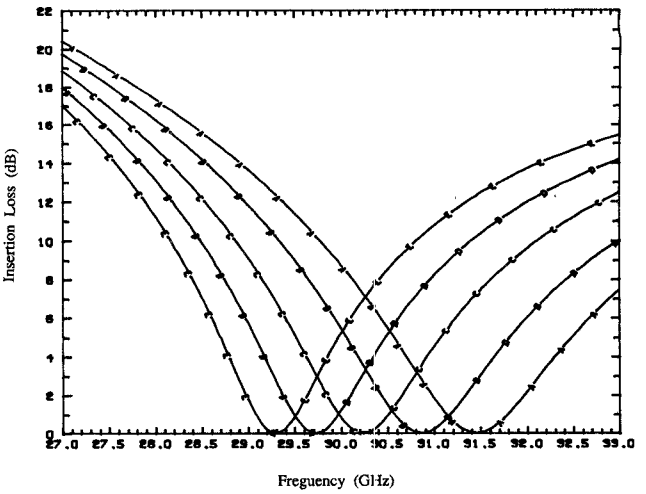

Fig. 9. Insertion loss of the filter versus frequency for different widths w of E-plane fin. $h1 = 1.753$ mm; $h2 = 0.127$ mm; $\epsilon_2 = 2.2$; $d = 1.483$ mm; $T = 2.0$ mm; $A: w = 0.1$ mm; $B: w = 0.2$ mm; $C: w = 0.3$ mm; $D: w = 0.4$ mm; $E: w = 0.5$ mm.

represents the evanescent-mode guide section, and it can be found in the same way as $\boldsymbol{S}_{T1}$. Since $\boldsymbol{S}_{d1}$, $\boldsymbol{S}_{d2}$, $\boldsymbol{S}_f$ and $\boldsymbol{S}_T$ are all known, the overall matrix $\boldsymbol{S}$, which characterizes the filter structure, can be determined from these scattering matrices by the generalized scattering matrix technique. The elements of the matrix $\boldsymbol{S}$ are given by

$$\begin{pmatrix} \boldsymbol{R}^{(1)} \\ \boldsymbol{R}^{(2)} \end{pmatrix} = \begin{pmatrix} \boldsymbol{S}_{11} & \boldsymbol{S}_{12} \\ \boldsymbol{S}_{21} & \boldsymbol{S}_{22} \end{pmatrix} \begin{pmatrix} \boldsymbol{I}^{(1)} \\ \boldsymbol{I}^{(2)} \end{pmatrix} \tag{37}$$

where the submatrices $\boldsymbol{S}_{11}$, $\boldsymbol{S}_{12}$, $\boldsymbol{S}_{21}$, and $\boldsymbol{S}_{22}$ are represented by

$$\boldsymbol{S}_{11} = \boldsymbol{S}_{d111} + \boldsymbol{S}_{d112}\boldsymbol{S}\boldsymbol{D}^{-1}\boldsymbol{S}\boldsymbol{U} \tag{38}$$

$$\boldsymbol{S}_{12} = \boldsymbol{S}_{d112} + \boldsymbol{S}\boldsymbol{D}^{-1}\boldsymbol{S}\boldsymbol{V} \tag{39}$$

$$\boldsymbol{S}_{21} = \boldsymbol{S}_{d112} + \boldsymbol{S}\boldsymbol{D}^{-1}\boldsymbol{S}\boldsymbol{P} \tag{40}$$

$$\boldsymbol{S}_{22} = \boldsymbol{S}_{d111} + \boldsymbol{S}_{d112}\boldsymbol{S}\boldsymbol{D}^{-1}\boldsymbol{S}\boldsymbol{Q} \tag{41}$$

$$\begin{aligned}\boldsymbol{S}\boldsymbol{D} = {} & (\boldsymbol{I} - \boldsymbol{S}_t\boldsymbol{S}_{f11}\boldsymbol{S}_t\boldsymbol{S}_{d122})(\boldsymbol{I} - \boldsymbol{S}_t\boldsymbol{S}_{f22}\boldsymbol{S}_t\boldsymbol{S}_{d211}) \\ & - \boldsymbol{S}_t\boldsymbol{S}_{f12}\boldsymbol{S}_t\boldsymbol{S}_{d211}\boldsymbol{S}_t\boldsymbol{S}_{f21}\boldsymbol{S}_t\boldsymbol{S}_{d122}\end{aligned} \tag{42}$$

$$\begin{aligned}\boldsymbol{S}\boldsymbol{U} = {} & \boldsymbol{S}_t\boldsymbol{S}_{f11}\boldsymbol{S}_t\boldsymbol{S}_{d121}(\boldsymbol{I} - \boldsymbol{S}_t\boldsymbol{S}_{f22}\boldsymbol{S}_t\boldsymbol{S}_{d211}) \\ & + \boldsymbol{S}_t\boldsymbol{S}_{f12}\boldsymbol{S}_t\boldsymbol{S}_{d211}\boldsymbol{S}_t\boldsymbol{S}_{f21}\boldsymbol{S}_t\boldsymbol{S}_{d121}\end{aligned} \tag{43}$$

$$\begin{aligned}\boldsymbol{S}\boldsymbol{V} = {} & \boldsymbol{S}_t\boldsymbol{S}_{f12}\boldsymbol{S}_t\boldsymbol{S}_{d212}(\boldsymbol{I} - \boldsymbol{S}_t\boldsymbol{S}_{f22}\boldsymbol{S}_t\boldsymbol{S}_{d211}) \\ & + \boldsymbol{S}_t\boldsymbol{S}_{f12}\boldsymbol{S}_t\boldsymbol{S}_{d211}\boldsymbol{S}_t\boldsymbol{S}_{f22}\boldsymbol{S}_t\boldsymbol{S}_{d212}\end{aligned} \tag{44}$$

$$\begin{aligned}\boldsymbol{S}\boldsymbol{P} = {} & (\boldsymbol{I} - \boldsymbol{S}_t\boldsymbol{S}_{f11}\boldsymbol{S}_t\boldsymbol{S}_{d122})\boldsymbol{S}_t\boldsymbol{S}_{f21}\boldsymbol{S}_t\boldsymbol{S}_{d121} \\ & + \boldsymbol{S}_t\boldsymbol{S}_{f11}\boldsymbol{S}_t\boldsymbol{S}_{d121}\boldsymbol{S}_t\boldsymbol{S}_{f21}\boldsymbol{S}_t\boldsymbol{S}_{d122}\end{aligned} \tag{45}$$

$$\begin{aligned}\boldsymbol{S}\boldsymbol{Q} = {} & (\boldsymbol{I} - \boldsymbol{S}_t\boldsymbol{S}_{f11}\boldsymbol{S}_t\boldsymbol{S}_{d122})\boldsymbol{S}_t\boldsymbol{S}_{f22}\boldsymbol{S}_t\boldsymbol{S}_{d212} \\ & + \boldsymbol{S}_t\boldsymbol{S}_{f12}\boldsymbol{S}_t\boldsymbol{S}_{d212}\boldsymbol{S}_t\boldsymbol{S}_{f21}\boldsymbol{S}_t\boldsymbol{S}_{d122}.\end{aligned} \tag{46}$$

III. Design Examples and Discussions

Several filters have been designed by the procedure described above. The design procedure can be used in a wide frequency range. However in this study, only band-

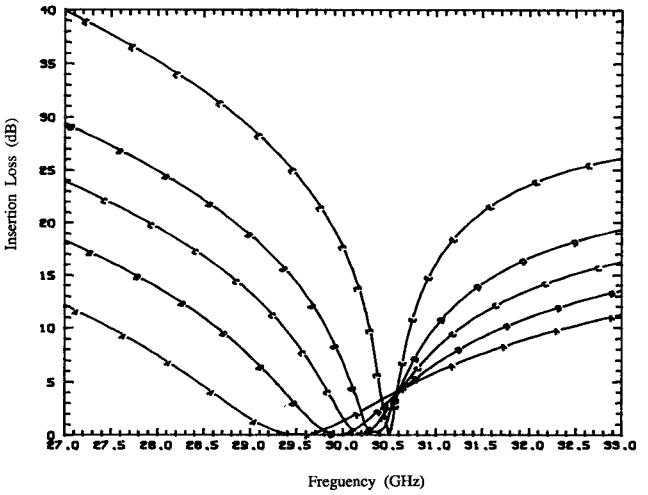

Fig. 10. Insertion loss of the filter versus frequency for different distances T between the step junction and the E-plane fin with Duriod substrate. $\epsilon_2 = 2.2$; $h1 = 1.753$ mm; $h2 = 0.127$ mm; $d = 1.50$ mm; $w = 0.3$ mm; $A:T = 1.5$ mm; $B:T = 2.0$ mm; $C:T = 2.5$ mm; $D:T = 3.0$ mm; $E:T = 4.0$ mm.

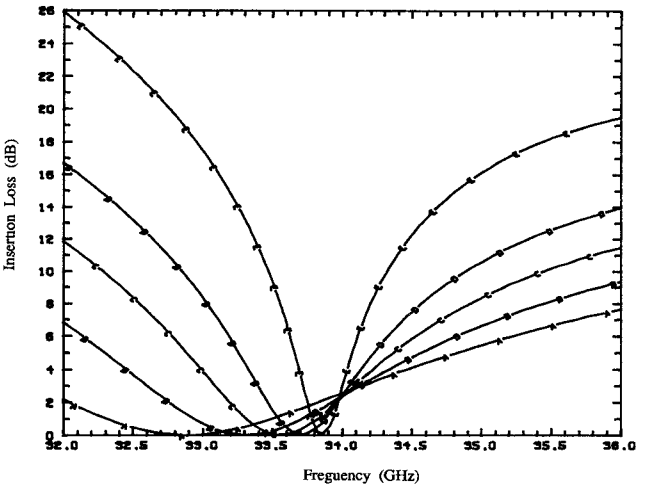

Fig. 11. Insertion loss of the filter versus frequency for different distances T between the step junmction and the E-plane fin (metal only). $d = 1.50$ mm; $w = 0.28$ mm; $A:T = 1.5$ mm; $B:T = 2.0$ mm; $C:T = 2.5$ mm; $D:T = 3.0$ mm; $E:T = 4.0$ mm.

pass filters operating in the *Ka*-band have been considered. In the following discussion, the larger waveguide is WR-28 (7.11 mm × 3.56 mm) while the smaller waveguide is WR-15 (3.76 mm × 1.88 mm). For accurate and efficient computation, the ratios of the modes have to be chosen such that $M/N = a_1/b_1$, $P/Q = a/b$, and $M/P = a_1/a$. In the following calculation, the numbers of modes used are $M = 8$, $N = 4$, $P = 4$, and $Q = 2$. The center frequency is the most important quantity for design of a bandpass filter. Attention is first directed to how the height and width of the single fin and the distance between the edge of the fin and the step junction affect the center frequency of the evanescent filter.

Fig. 8 shows the relationship between the height of the fin and center frequency for a filter with the E-plane fin supported by a Duroid substrate (dielectric constant $\epsilon = 2.2$, thickness $h2 = 0.127$ mm). The center frequency decreases as the height d of the fin increases, because as d increases there is more electric energy stored in the gap between the fin and the wall of the guide. This corresponds to a larger shunt capacitor in its equivalent network while the series inductance X_1 exhibits little change.

Fig. 9 shows the relationship between the width of the fin and the central frequency for a fin with a fixed height. The wider the fin, the lower the center frequency. The wider fin leads to a larger capacitance and inductance in its equivalent circuit and hence a lower resonant frequency (see Fig. 4(d)).

The insertion loss versus the frequency for different distance T of the filter with fixed width and height of the fin is shown in Figs. 10 and 11. In Fig. 10 the fin is supported by a Duroid substrate while in Fig. 11 there is no dielectric substrate. When the fin is separated from the step junction, the center frequency becomes higher and the curve becomes steeper, since the coupling between the fin and the step becomes weaker.

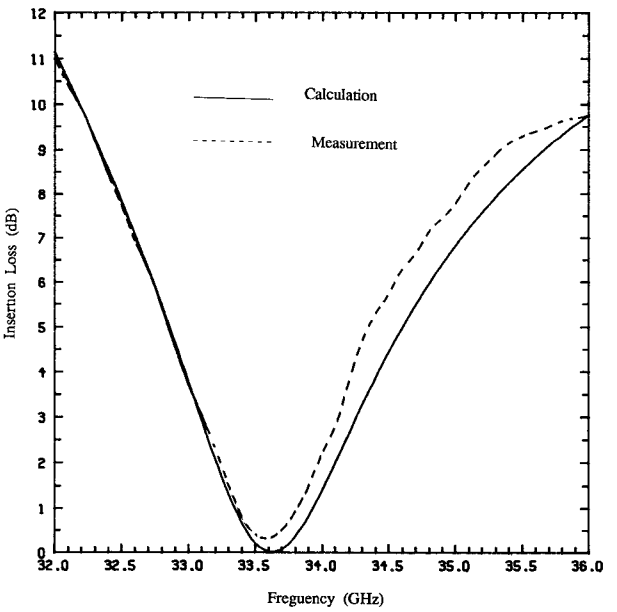

Fig. 12. Computed and measured insertion loss for an evanescent-mode waveguide filter with an E-plane fin (metal only, $h_1 = 1.753$ mm, $h_2 = 0.157$ mm, $d = 1.511$ mm, $w = 0.287$ mm, $T = 2.506$ mm).

With the data presented above, it is now possible to design a filter with one fin element. Fig. 12 shows the results for a filter designed in the *Ka*-band using one fin element without a dielectric layer. The solid curve represents the results obtained by this analysis and the dashed line indicates the meassured data. They are in good agreement. Fig. 13 shows the results of the filter with the E-plane fin supported by a Duroid layer. Once again agreement between theoretical prediction and experimental data is quite good. The small deviation of the insertion loss between theory and experiment at the center frequency comes from the metal and dielectric loss.

Fig. 14 shows the calculated response of a filter that consists of two equal E-plane fin elements on a Duroid

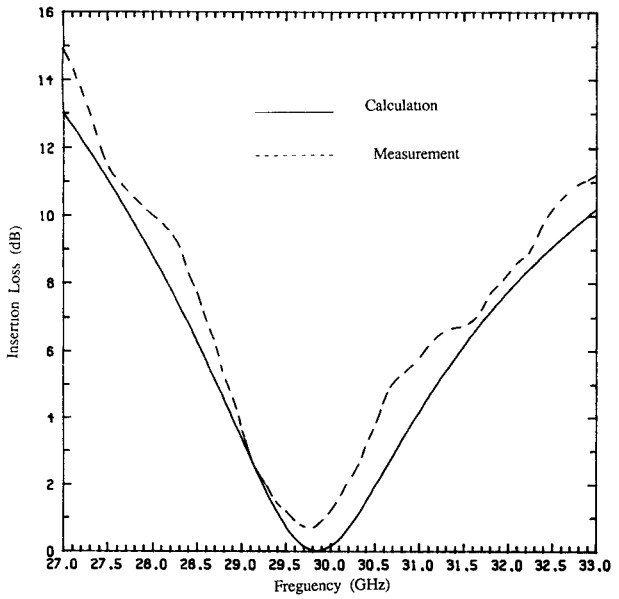

Fig. 13. Computed and measured insertion loss for an evanescent-mode waveguide filter with an E-plane fin on a Duroid substrate ($h_1 = 1.753$ mm, $\epsilon_2 = 2.2$, $h_2 = 0.157$ mm, $d = 1.483$ mm, $w = 0.292$ mm, $T = 1.502$ mm).

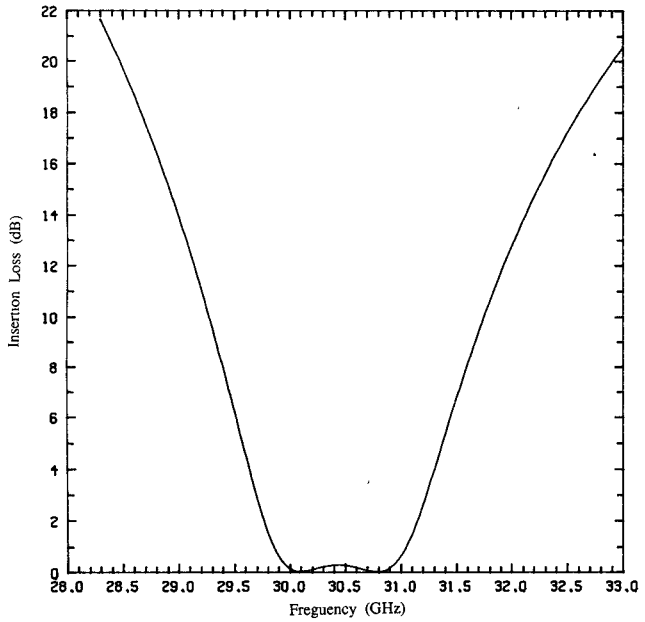

Fig. 14. Insertion loss for an evanescent-mode waveguide filter with two E-plane fins on a Duroid substrate ($h_1 = 1.753$ mm, $h_2 = 0.127$ mm, $d = 1.50$ mm, $w = 0.292$ mm, $T = 2.0$ mm, $T1 = 4.6248$ mm, $\epsilon_2 = 2.2$).

substrate. The height of the fin, the distance from the edge of the fin to the double-step junction, and the spacing of the two fins are the design parameters. The 3-dB bandwidth is about 1.6 GHz. It is noted that the steepness of the out-of-band insertion loss curve on the higher frequency side in Fig. 14 is almost equal to the one on the lower frequency side. This happens because the waveguide below its cutoff frequency acts like a lumped reactance.

In general, wider bandwidth and better transmission performance can be achieved by increasing the number of fins. For a multifin structure an optimization procedure similar to [16] may be used to optimize the performance of the filter. Alternatively, a filter synthesis can be used to find the required equivalent circuit parameters in the filter. The necessary fin dimensions and fin spacing can be found from a look-up table. The center frequency can be controlled by the dimensions of the fins and the distance between the edge of the fin and the double-step junction. The shorter the height and the narrower the width, the higher the center frequency. Also a longer distance from the edge of the fin to the double-step junction leads to a higher central frequency. The height of the fin is the most sensitive parameter to the center frequency. For instance, in Fig. 9, if the width of the fin changes by 0.1 mm, the center frequency shifts about 0.5 GHz, while a variation of 0.05 mm on the height corresponds to a frequency change of about 1 GHz (see Fig. 8). Since the nontouching fins can be produced by photolithographic techniques, fine tuning is normally not required.

IV. Conclusions

A computer-aided design algorithm for an evanescent-mode waveguide filter with nontouching E-plane fins is presented. In this design, the fundamental mode as well as the higher order mode effects have been taken into account. This is important in an accurate filter design. The filter designed in *Ka*-band has been tested and good agreement between the measurement and the theory is observed. It is believed that this kind of filter will be useful in the millimeter-wave frequency region.

References

[1] E. T. Jaynes, "Ghost modes in imperfect waveguides," *Proc. IRE*, vol. 46, pp. 416–418, Feb. 1958.

[2] W. A. Edson, "Microwave filters using ghost-mode resonance, in *Proc. IRE Electron. Components Conf.*, vol. 19, 1961, pp. 2.

[3] G. Craven, "Waveguide band-pass filters using evanescent modes," *Electron. Lett.*, vol. 2, pp. 251–252, 1966.

[4] G. Craven and C. K. Mok, "The design of evanescent mode waveguide band-pass filters for a prescribed insertion loss characteristic," *IEEE Trans. Microwave Theory Tech.*, vol. MTT-19, pp. 295–308, Mar. 1971.

[5] R. Synder, "New Application of evanescent mode waveguide to filters design," *IEEE Trans. Microwave Theory Tech.*, vol. MTT-25, pp. 1013–1021, Dec. 1977.

[6] C. K. Mok, "Diaphragms in evanescent waveguides," *Electron. Lett.*, vol. 4, pp. 43–44, Feb. 1968.

[7] Q. Zhang and T. Itoh, "Spectral-domain analysis of scattering from E-plane circuit elements," *IEEE Trans. Microwave Theory Tech.*, vol. MTT-35, pp. 138–150, Feb. 1987.

[8] S. B. Cohn, "Direct-coupled-resonator filters," *Proc. IRE*, vol. 2, pp. 187–196, Feb. 1957.

[9] G. L. Mattaei, L. Young, and E. M. T. Jones, *Microwave Filters, Impedance-Matching Networks, and Coupling Structures*. New York: McGraw-Hill, 1964, ch. 8.

[10] J. Pace and R. Mittra, "Generalized scattering matrix analysis of waveguide discontinuity problem," in *Quasi-Optics XIV*. New York: Brookline Press, 1964, pp. 172–194.

[11] R. Mittra and S. W. Lee, *Analytical Techniques in the Theory of Guided Waves*. New York: Macmillan, 1971, pp. 207–217.

[12] H. Patzelt and F. Arndt, "Double-plane steps in rectangular waveguide and their application for transformer, irises, and filters," *IEEE Trans. Microwave Theory Tech.*, vol. MTT-30, pp. 771–776, May 1982.

[13] T. K. Chu, T. Itoh, and Y. C. Shih, "Comparative study of mode-matching formulations for microstrip discontinuity problems," *IEEE Trans. Microwave Theory Tech.*, vol. MTT-33, pp. 1018–1023, Oct. 1985.
[14] R. F. Harrington, *Time-Harmonic Electromagnetic Fields*. New York, McGraw-Hill, 1968.
[15] F. Arndt and T. Wriedt, "Computer-optimized multisection transformers between rectangular waveguide of adjacent frequency bands," *IEEE Trans. Microwave Theory Tech.*, vol. MTT-32, pp. 1479–1484, Nov. 1984.
[16] Y. C. Shih, T. Itoh, and L. Q. Bui, "Computer-aided design of millimeter wave *E*-plane filter," *IEEE Trans. Microwave Theory Tech.*, vol. MTT-31, pp. 135–142, Feb. 1983.

✠

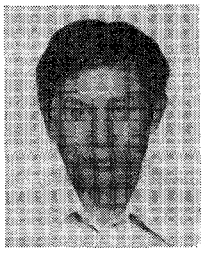

Qiu Zhang was born on October 19, 1941, in Nanchang, China. He graduated from the Jiangxi University in 1966. He received the M.S. and Ph.D. degrees in electrical engineering from the University of Texas at Austin in 1984 and 1987, respectively. He is currently working in the Fusion Research Center in the Physics Department at the University of Texas at Austin. His current interests are the analysis and design of microwave printed circuit components.

Tatsuo Itoh (S'69–M'69–SM'74–F'82) received the Ph.D. degree in electrical engineering from the University of Illinois, Urbana, in 1969.

From September 1966 to April 1976, he was with the Electrical Engineering Department, University of Illinois. From April 1976 to August 1977, he was a Senior Research Engineer in the Radio Physics Laboratory, SRI International, Menlo Park, CA. From August 1977 to June 1978, he was an Associate Professor at the University of Kentucky, Lexington. In July 1978, he joined the faculty at the University of Texas at Austin, where he is now a Professor of Electrical and Computer Engineering and Director of the Electrical Engineering Research Laboratory. During the summer of 1979, he was a guest researcher at AEG-Telefunken, Ulm, West Germany. Since September 1983, he has held the Hayden Head Centennial Professorship of Engineering at the University of Texas. Since September 1984, he has been the Associate Chairman for Research and Planning in the Electrical and Computer Engineering Department.

Dr. Itoh is a member of the Institute of Electronics and Communication Engineers of Japan, Sigma Xi, and Commissions B and D of USNC/URSI. He served as the Editor of IEEE TRANSACTIONS ON MICROWAVE THEORY AND TECHNIQUES for 1983–1985. He serves on the Administrative Committee of the IEEE Microwave Theory and Techniques Society. Dr. Itoh is a Professional Engineer registered in the state of Texas.